TEKTONIKA

Supporting Information
for

Brittle-ductile Coupling and Block Rotation During Rifting Revealed Through Digital Volume Correlation Analysis of a Crustal-scale Analogue Experiment

Timothy C. Schmid[*1], Jürgen Adam[2], Frank Zwaan[1,3,4], Guido Schreurs[1], Dave Hollis[5]

[1]*Institute of Geological Sciences, University of Bern, Switzerland*
[2]*Department of Earth Sciences, Royal Holloway University London, England*
[3]*Helmholtz Centre Potsdam – GFZ German Research Centre for Geosciences, Potsdam, Germany*
[4]*Department of Geosciences, University of Fribourg, Switzerland*
[5]*LaVision UK Ltd, England*

[*]*Corresponding author: Timothy Schmid (timothy.schmid@unibe.ch)*

SI-1. Analogue modelling materials

The models presented in Zwaan et al. (2018a) involve brittle and viscous materials, representing the brittle upper and a ductile lower crust. The upper brittle layer of the analogue models consists of fine dry quartz sand (grain size 60 – 205 µm) with a bulk density of 1560 kg m^{-3}. This density is achieved by sieving sand into the model box from a height of ca. 30 cm or more (Schmid et al., 2020b). Granular materials such as quartz sand are generally characterized by elastic-plastic behavior. Increasing stress initially causes strain-hardening until failure at peak strength. A subsequent drop in material strength allows the system to attain a state of dynamic stable sliding (Lohrmann et al., 2003). The quartz sand used in Zwaan et al. (2018a) has an angle of internal peak friction of 36° (i.e., coefficient of peak friction µ = 0.73) and an angle of internal dynamic-stable friction of 31° (i.e., coefficient of dynamic stable friction µ = 0.61; Zwaan et al., 2018b), which are close to typical values for upper crustal rocks (Schellart and Strak, 2016). The cohesion of the sand is almost negligible at 9 ± 98 Pa (Zwaan et al., 2018b), so that it is a proper material to simulate the upper crust (e.g., Abdelmalak et al., 2016).

Dilation and localized deformation in the quartz sand locally lowers the peak friction coefficient over time, resulting in strain softening of about 16 % (i.e., the difference between the coefficient of peak friction and dynamic friction coefficient normalized by the coefficient of peak friction; Panien et al., 2006b) obtained from mutual two-point regression analysis (Santimano et al., 2015). Note that, sand does not form true discrete "faults". Instead, "shear zones" develop, because of sand dilation due to sand grains moving along each other during deformation (Panien et al., 2006a and references therein). This density difference causes the faults to appear on XRCT scans (Colletta et al., 1991). Additionally, during model preparation sand layers are flattened every 1 cm with a scraper causing local density variations, that are

visible on XRCT images, but are not regarded as significantly influencing the model results (Zwaan et al., 2018a).

The viscous material that forms the lower part of the model, simulating the lower crust consists of a mixture of corundum sand (grain size 88 – 175 µm, $\rho_{specific}$ = 3960 kg m^{-3}) and polydimethylsiloxane (PDMS, $\rho_{specific}$ = 965 kg m^{-3}) with a mixing ratio 1:1 to achieve a density of 1600 kg m^{-3}. The brittle-viscous setup thus has a density gradient increasing with depth avoiding density instabilities and spontaneous upwelling of the viscous lower layer. The viscous mixture has a viscosity of $1.5 \cdot 10^5$ Pa and a stress exponent of ~1.06 – 1.10 (Zwaan et al., 2018c) but the material behavior remains near-Newtonian for model strain rates below 10^{-4} s^{-1}.

For the DVC analysis (Adam et al., 2013; Schmid et al., 2022; Zwaan et al., 2018a), small quantities (weight ratio 1:50) of high-density Zirshot ceramic microbeads (grain size 150-210 µm, $\rho_{specific}$ = 3800 kg m^{-3}) are mixed with the quartz and corundum sands to enhance volumetric patterns on XRCT scans to facilitate correlation of intensity patterns. Zirshot grains produce volumetric patterns in the 3D XRCT data and are subsequently traced and quantified with the applied DVC algorithms. The influence of such ceramic microbeads on the overall mechanical properties is minor and thus can be neglected (Klinkmüller, 2011; Panien et al., 2006b; Schmid et al., 2020a, b). Properties of all materials are listed in table SI-1.

Table SI-1: Material properties. Quartz sand density denoted with * is achieved by sieving from 30 cm height or more.

Granular materials	Quartz sand	Corundum sand	Zirshot	Viscous material	PDMS/corundum mixture
Density (kg m^{-3})	1560*	3960	3800	Density (kg m^{-3})	1600
Grainsize (µm)	60-250	88-175	150-210	Viscosity (Pa s)	1.5 x 10^5
Peak Friction angle an coefficient µ	36° - 0.73	37° - 0.75	-	Stress exponent n	1.06 – 1.10
Strain softening (%)	16	17	-		
Cohesion (Pa)	9 ± 98	39 ± 10	-		

SI-2. Scaling of analogue materials

For scaling purposes, the standard equations based on (Hubbert, 1937) are applied to ensure proper scaling of stresses in analogue models up to natural scales:

$$\sigma^* = \rho^* g^* h^* \qquad \text{(eq. SI-1)}$$

By convention, σ^* is defined as: $\sigma^* = \frac{\sigma^m}{\sigma^n}$, with m and n indicating values for model and nature, respectively. Further, ρ^*, g^*, h^* and η^* denote density, gravity, length, and viscosity ratios, respectively. With the stress ratio and the viscosity ratio η^* the strain rate ratio $\dot{\varepsilon}^*$ can be derived (Schellart and Strak, 2016 and references therein):

$$\dot{\varepsilon}^* = \frac{\sigma^*}{\eta^*} \qquad \text{(eq. SI-2).}$$

Subsequently, the value of σ^* allows to compute the velocity ratio v^* and time ratio t^* by means of equation SI-3:

$$\dot{\varepsilon}^* = \frac{v^*}{h^*} = \frac{1}{t^*} \qquad \text{(eq. SI-3)}$$

The viscosity of the lower crust can vary significantly (e.g., Buck, 1991), but assuming a viscosity value of 10^{21} Pa s for the natural example with a background strain rate of $\dot{\varepsilon} = 10^{14}$ s^{-1} (Shinevar et al., 2015), one hour in the model translates to ~0.8 Myr in nature. It follows that

the applied divergence velocity of 7.5 mm h^{-1} represents a divergence velocity of ~5 mm yr^{-1} in nature, which is close to values obtained by GNSS-based plate motion studies of natural continental rift systems (a few mm yr^{-1}; e.g., Saria et al., 2014). The applied divergence velocity field translates to a background strain rate of ~7 10^{-6} s^{-1} in the model, which is (using eq. SI-3) equivalent to a background strain rate of 10^{-15} s^{-1} in nature. Compared to the background strain rate of 10^{-14} s^{-1} from Shinevar et al. (2015), scaling factors from Zwaan et al. (2018a) yield a background strain rate one magnitude smaller (i.e., 10^{-15} s^{-1}). However, the calculated value is still within the range of documented lower crustal strain rates (e.g., Fagereng and Biggs, 2019 and references therein). The chosen value in Shinevar et al. (2015) reflects a uniform crustal strain rate but in nature, localized deformation may cause strain rates ≥ 10^{-14} s^{-1}, while the effective background strain remains below 10^{-14} s^{-1}. All parameters used for scaling are listed in Table SI-2.

Dynamic similarities between model and natural prototype are ensured by comparing the dimensionless Smoluchowski number S_m, the Ramberg number R_m and, the Reynolds number R_e. S_m is the ratio between gravitational stress and cohesive strength (Ramberg, 1981) $S_m = \frac{\rho g h}{C+\mu\rho g h}$, where ρ, g, h, C, and μ are the density, gravitational acceleration, thickness, cohesion and, friction coefficient, respectively. R_m is defined as $R_m = \frac{\rho g h^2}{\eta v}$, where η and v are further the viscosity and extension velocity, respectively. Finally, R_e is defined as the ratio between inertial forces to viscous forces with $R_e = \frac{\rho v h}{\eta}$.

Table SI-2: Scaling parameters, scaling factors, and dimensionless numbers for the crustal-scale model setup and nature.

	General parameters			Brittle upper crust		Ductile lower crust		Dimensionless numbers		
	Gravity [m s^{-2}]	Crustal thickness [m]	Divergence velocity [m s^{-1}]	Density [kg m^{-3}]	Cohesion [Pa]	Density [kg m^{-3}]	Viscosity [Pa s]	Smoluchowski Sm	Ramberg Rm	Reynolds Re
Model	9.81	$8\ 10^{-2}$	$2.1\ 10^{-6}$	1560	9	1600	$1.5\ 10^{5}$	1	80	<<1
Nature	9.81	$4\ 10^{4}$	$1.3\ 10^{-10}$	2800	$5\ 10^{7}$	2900	10^{21}	1	81	<<1
Scaling factors $x^* = x^m/x^n$ [dimensionless]										
	σ^*	ρ^*	g^*	h^*	c^*	$\dot{\varepsilon}^*$	η^*	v^*	t^*	
	$1\ 10^{-6}$	0.56	1	$2\ 10^{-6}$	$2\ 10^{-6}$	$6.7\ 10^{9}$	$1.5\ 10^{-16}$	$1.3\ 10^{4}$	$1.5\ 10^{-10}$	

SI-3. Incremental displacement components

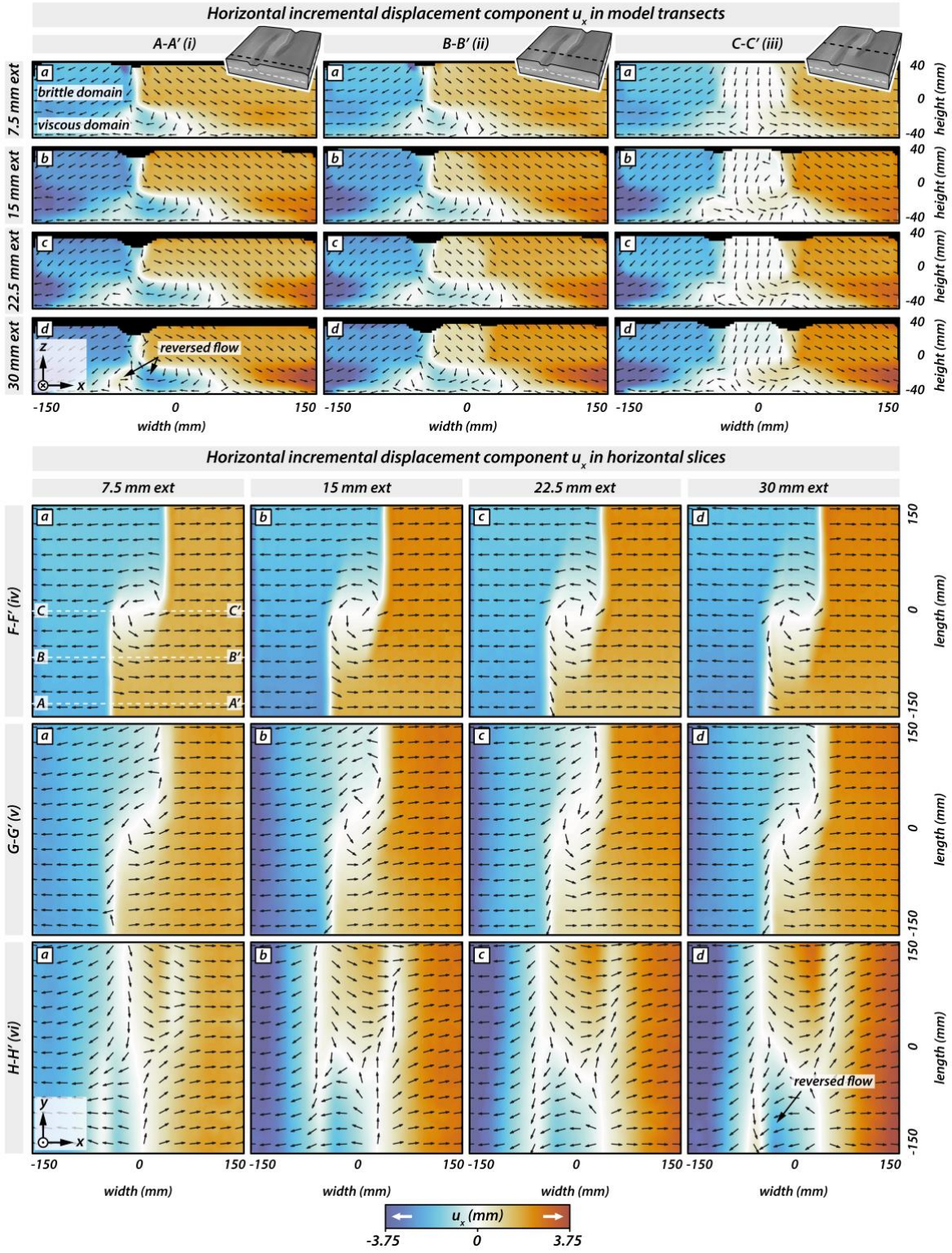

Figure SI-1: *Incremental DVC maps of the horizontal displacement component u_X at distinct model positions. The upper and lower parts correspond to rift transects A-A', B-B' and C-C', and horizontal slices F-F' (i.e., brittle layer), G-G' (i.e., brittle-viscous interface) and H-H' (i.e., viscous layer), respectively. Vectors indicate the 3D displacement field projected onto the xz-, and xy-plane, respectively (vectors have all unit lengths for better visibility). White lines indicate zero-displacement.*

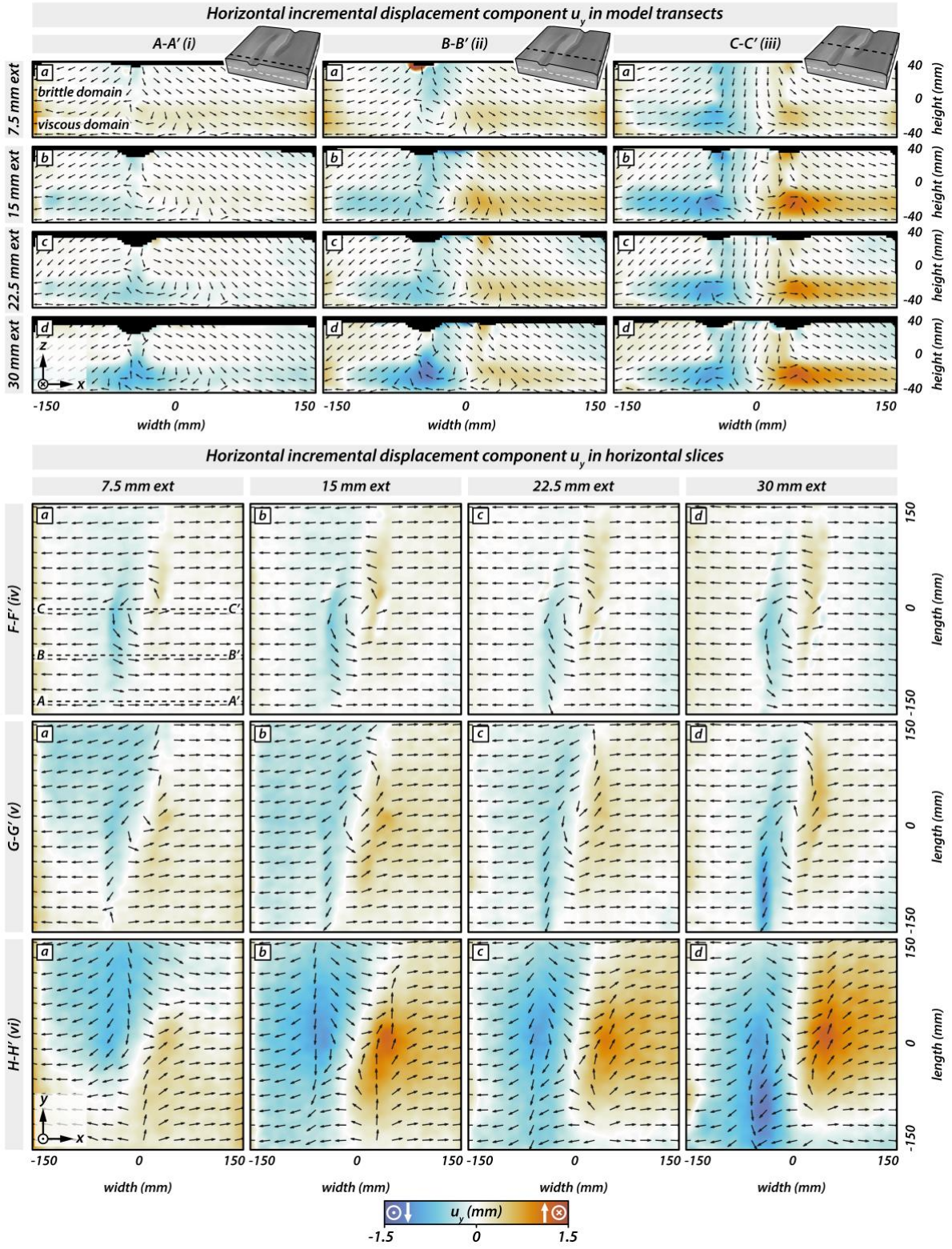

Figure SI-2: *Incremental DVC maps of the horizontal displacement component u_y. The upper and lower parts correspond to rift transects A-A', B-B', and C-C', and horizontal slices F-F' (i.e., brittle layer), G-G' (i.e., brittle-viscous interface) and H-H' (i.e., viscous layer), respectively. Vectors indicate the 3D displacement field projected onto the xz- and xy-plane, respectively (vectors have all unit lengths for better visibility). Direction markers in the color bar indicate directions in transects (outer markers) and horizontal slices (inner markers). White lines indicate zero-displacement.*

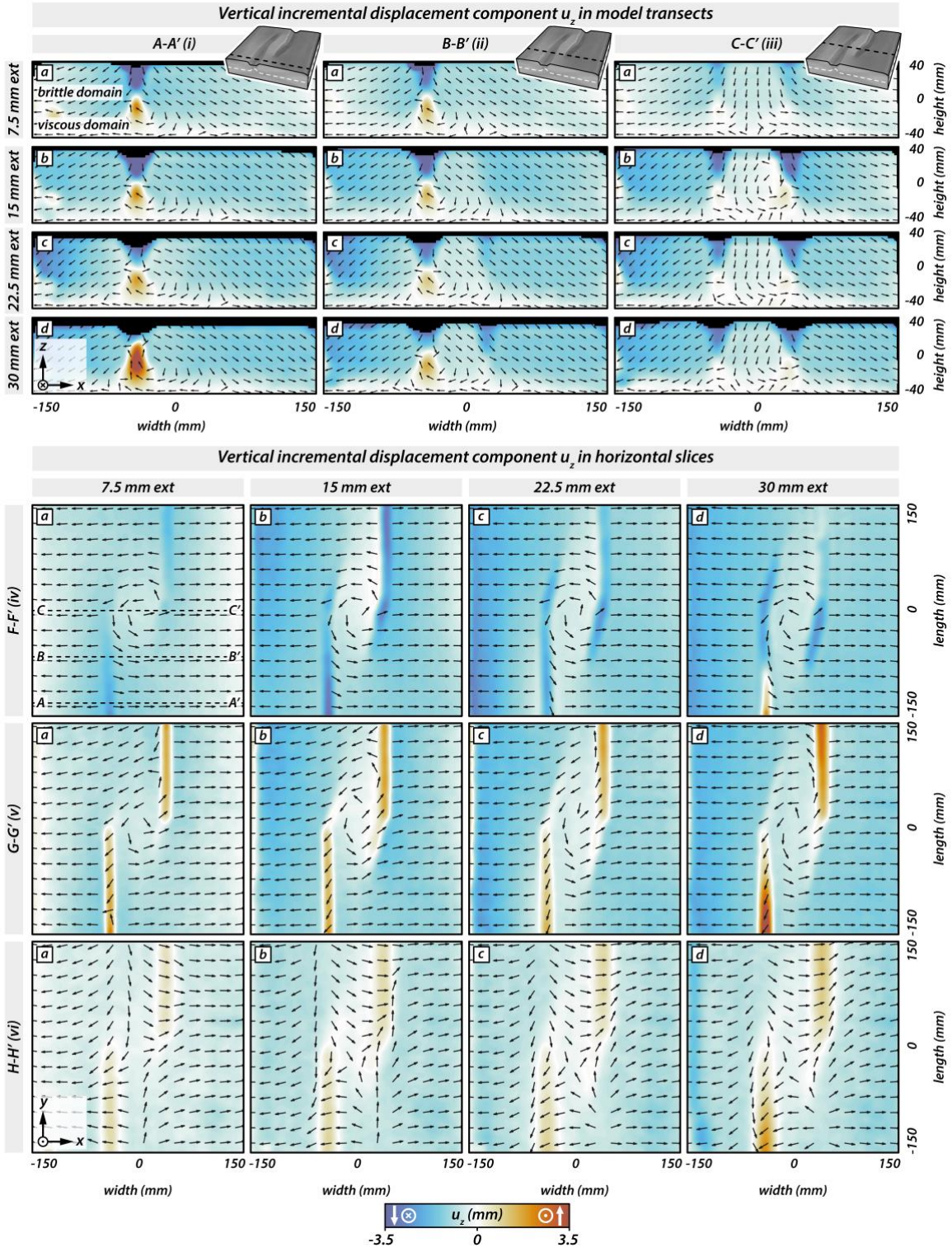

Figure SI-3: *Incremental DVC maps of the vertical displacement component u_z. The upper and lower parts correspond to rift transects A-A', B-B' and C-C', and horizontal slices F-F' (i.e., brittle layer), G-G' (i.e., brittle-viscous interface) and H-H' (i.e., viscous layer), respectively. Vectors indicate the 3D displacement field projected onto the xz- and xy-plane, respectively (vectors have all unit lengths for better visibility). Direction markers in the color bar indicate directions in transects (outer markers) and horizontal slices (inner markers). White lines indicate zero-displacement.*

References

Abdelmalak, M., Bulois, C., Mourgues, R., Galland, O., Legland, J.-B., Gruber, C., 2016. Description of new dry granular materials of variable cohesion and friction coefficient: Implications for laboratory modeling of the brittle crust. Tectonophysics 684, 39-51.
https://doi.org/10.1016/j.tecto.2016.03.003

Adam, J., Klinkmüller, M., Schreurs, G., Wieneke, B., 2013. Quantitative 3D strain analysis in analogue experiments simulating tectonic deformation: Integration of X-ray computed tomography and digital volume correlation techniques. Journal of Structural Geology 55, 127-149.
https://doi.org/10.1016/j.jsg.2013.07.011

Buck, W.R., 1991. Modes of continental lithospheric extension. Journal of Geophysical Research: Solid Earth 96, 20161-20178.
https://doi.org/10.1029/91JB01485

Colletta, B., Letouzey, J., Pinedo, R., Ballard, J.F., Balé, P., 1991. Computerized X-ray tomography analysis of sandbox models: Examples of thin-skinned thrust systems. Geology 19, 1063-1067.
https://doi.org/10.1130/0091-7613(1991)019<1063:CXRTAO>2.3.CO;2

Fagereng, Å., Biggs, J., 2019. New perspectives on 'geological strain rates' calculated from both naturally deformed and actively deforming rocks. Journal of Structural Geology 125, 100-110.
https://doi.org/10.1016/j.jsg.2018.10.004

Hubbert, M.K., 1937. Theory of scale models as applied to the study of geologic structures. Geological Society of America Bulletin 48, 1459-1520.
https://doi.org/10.1130/GSAB-48-1459

Klinkmüller, M., 2011. Properties of analogue materials, experimental reproducibility and 2D/3D deformation quantification techniques in analogue modelling of crustal-scale processes. PhD Thesis, University of Bern, Switzerland.

Lohrmann, J., Kukowski, N., Adam, J., Oncken, O., 2003. The impact of analogue material properties on the geometry, kinematics, and dynamics of convergent sand wedges. Journal of Structural Geology 25, 1691-1711.
https://doi.org/10.1016/S0191-8141(03)00005-1

Panien, M., Buiter, S., Schreurs, G., Pfiffner, O.-A., 2006a. Inversion of a symmetric basin: insights from a comparison between analogue and numerical experiments. Geological Society, London, Special Publications 253, 253-270.
https://doi.org/10.1144/GSL.SP.2006.253.01.13

Panien, M., Schreurs, G., Pfiffner, A., 2006b. Mechanical behaviour of granular materials used in analogue modelling: insights from grain characterisation, ring-shear tests and analogue experiments. Journal of Structural Geology 28, 1710-1724.
https://doi.org/10.1016/j.jsg.2006.05.004

Ramberg, H., 1981. Gravity, deformation and the earth's crust: in theory, experiments and geological application. Academic press.

Santimano, T., Rosenau, M., Oncken, O., 2015. Intrinsic versus extrinsic variability of analogue sand-box experiments–Insights from statistical analysis of repeated accretionary sand wedge experiments. Journal of Structural Geology 75, 80-100.
https://doi.org/10.1016/j.jsg.2015.03.008

Saria, E., Calais, E., Stamps, D., Delvaux, D., Hartnady, C., 2014. Present-day kinematics of the East African Rift. Journal of Geophysical Research: Solid Earth 119, 3584-3600.
https://doi.org/10.1002/2013JB010901

Schellart, W.P., Strak, V., 2016. A review of analogue modelling of geodynamic processes: Approaches, scaling, materials and quantification, with an application to subduction experiments. Journal of Geodynamics 100, 7-32.
https://doi.org/10.1016/j.jog.2016.03.009

Schmid, T., Schreurs, G., Warsitzka, M., Rosenau, M., 2020a. Effect of sieving height on density and friction of brittle analogue material: Ring-shear test data of corundum sand used for analogue experiments in the Tectonic Modelling Lab of the University of Bern (CH). GFZ Data Services.
https://doi.org/10.5880/fidgeo.2020.005

Schmid, T., Schreurs, G., Warsitzka, M., Rosenau, M., 2020b. Effect of sieving height on density and friction of brittle analogue material: ring-shear test data of quarz sand used for analogue experiments in the Tectonic Modelling Lab of the University of Bern. GFZ Data Services.
https://doi.org/10.5880/fidgeo.2020.006

Schmid, T.C., Schreurs, G., Adam, J., 2022. Rotational extension promotes coeval upper crustal brittle faulting and deep-seated rift-axis parallel flow: Dynamic coupling processes inferred from analogue model experiments. Journal of Geophysical Research: Solid Earth, e2022JB024434.
https://doi.org/10.1029/2022JB024434

Shinevar, W.J., Behn, M.D., Hirth, G., 2015. Compositional dependence of lower crustal viscosity. Geophysical Research Letters 42, 8333-8340.
https://doi.org/10.1002/2015GL065459

Zwaan, F., Schreurs, G., Adam, J., 2018a. Effects of sedimentation on rift segment evolution and rift interaction in orthogonal and oblique extensional settings: Insights from analogue models analysed with 4D X-ray computed tomography and digital volume correlation techniques. Global and planetary change 171, 110-133.
https://doi.org/10.1016/j.gloplacha.2017.11.002

Zwaan, F., Schreurs, G., Gentzmann, R., Warsitzka, M., Rosenau, M., 2018b. Ring-shear test data of quartz sand from the Tectonic Modelling Lab of the University of Bern (CH). GFZ Data Services.
https://doi.org/10.5880/fidgeo.2018.028

Zwaan, F., Schreurs, G., Ritter, M., Santimano, T., Rosenau, M., 2018c. Rheology of PDMS-corundum sand mixtures from the Tectonic Modelling Lab of the University of Bern (CH). GFZ Data Services.
https://doi.org/10.5880/fidgeo.2018.023